International Journal of Automotive Technology, Vol. 13, No. 1, pp. 97−107 (2012)
DOI 10.1007/s12239−012−0009−4

1229−9138/2012/062−09

DYNAMIC ANALYSIS OF SPIRAL BEVEL GEARED ROTOR SYSTEMS APPLYING FINITE ELEMENTS AND ENHANCED LUMPED PARAMETERS

X. HUA, T. C. LIM*, T. PENG and W. E. WALI

Vibro-Acoustics and Sound Quality Research Laboratory, School of Dynamic Systems, Mechanical Engineering, 598 Rhodes Hall, P.O. Box 210072, University of Cincinnati, Cincinnati, OH 45221-0072, USA

(Received 16 August 2011; Revised 19 September 2011)

ABSTRACT−The dynamics of spiral bevel gears like most high-speed precision gears employed in motor vehicles and off highway equipments are substantially affected by the structural characteristics of the shafts and bearings. The lumped parameter model is one of the common tools applied to perform gear dynamic analysis. Even though the lumped parameter approach is computationally fast and conveniently efficient, it typically uses limited number of coordinates and may not fully account for the shaft-bearing structural characteristics accurately. In this analysis, the finite element formulation, that can generally represent more complete characteristics of the shaft-bearing assembly, is employed to enhance the current lumped parameter synthesis theory using the concept of effective mass and inertia elements. Computational output shows that the enhanced lumped parameter synthesis model is capable of predicting sufficiently accurate dynamic response when compared to the direct dynamic finite element calculations, and much more precise response than previous lumped parameter results, especially when the gear dynamics are associated with the pinion or gear bending modes. Even though this analysis focuses primarily on the spiral bevel geared rotor systems, the proposed methodology and analysis results can be easily extended to other types of gears.

KEY WORDS : Spiral bevel gears, Gear dynamics, Enhanced lumped parameters, Dynamic finite elements

1. INTRODUCTION

As design of geared-based powertrain systems become more compact, the dynamics of high speed geared rotor systems becomes a more critical factor to generated acoustic noise and structural durability. Under dynamic conditions, the meshing force acting on the gear teeth is amplified leading to potential reduction in the gear fatigue life and allowing transmission of large amplitude vibratory response to the housing causing gear whine. To be able to design quieter and more durable gearboxes, we have to develop an in-depth understanding of the structural dynamics responsible for excitation and dynamic response. Hence, an approach that can accurately predict gear dynamic response and be able to provide an in-depth understanding of the underlying physics controlling the vibration and acoustic noise generation is highly desirable.

The dynamics of geared rotor systems have been studied extensively in the past (Ozguven and Houser, 1998; Smith, 2003, Vedmar and Andersson, 2003; Tamminana *et al*., 2007; Iida *et al*., 1985; Kubur *et al*., 2004; Vinayak *et al*., 1995; Lim and Li, 1999; Lim and Singh, 1991; Lim and Houser, 1997) . However, most of the studies are focused on parallel axis gears. Even though a lot is now known about the dynamical characteristics of parallel axis geared rotor systems, the results have not been applied much to analyze the response of non-parallel axis geared rotor systems such as straight and spiral bevel gears. Only in recent years that the study of the dynamics of spiral bevel geared rotor systems have gained some attention (Cheng, 2000; Peng and Lim, 2009a, 2009b, 2007c). For instance, Cheng and Lim (Cheng, 2000) developed the single-point gear mesh-coupling model based on the exact spiral bevel gear geometry. This mesh model is then applied to develop multiple degrees of freedom, lumped parameter model of the spiral bevel geared rotor system. Later, by using this same model, Peng and Lim (Peng and Lim, 2009a, 2009b, 2007c) investigated the influence of various gear system parameters on the dynamic characteristics of the spiral bevel geared rotor system. However, due to the limited number of degrees of freedom employed, the lumped parameter model cannot fully take into the account of the shaft-bearing dynamic characteristics. Moreover, the lumped parameter synthesis method used in the proposed model, which is the key to representing shaft-bearing structural characteristics, is quite primitive. Current lumped parameter approach is fundamentally deficient and unable to reasonably compute the values of effective lumped

**Corresponding author*. e-mail: teik.lim@uc.edu

mass, inertia and stiffness properties of the pinion and gear.

In this study, two modeling methods of spiral bevel geared rotor dynamic system, which are the dynamic finite element modeling and the enhanced equivalent lumped parameter synthesis, are introduced and compared. This first objective of this paper is to develop a dynamic finite element model that can better take into account and describe the shaft-bearing dynamic characteristics as compared to the existing multiple degrees of freedom, lumped parameter dynamic approach (Cheng, 2000) . The second objective is to develop a more accurate lumped point parameter synthesis method by considering the shaft-bearing structural characteristics employed in previous lumped parameter model (Cheng, 2000) and compare the results with the proposed dynamic finite element model.

2. DYNAMIC FINITE ELEMENTS

As shown in Figure 1, the mass and inertia elements for each of the pinion head and the ring gear is lumped at one node, and these two nodes are coupled via a mesh stiffness between them. The mass and inertia elements of the differential assembly are also lumped at one node. The pinion shaft and gear shaft are modeled with beam elements, for which consistent mass matrix is used. The bearings are modeled as stiffness matrices according to a bearing stiffness formulation (Lim and Singh, 1990a, 1990b). The engine and load are each represented by one node. All nodes of the system have 6 Cartesian coordinates except for the two nodes representing the engine and load that only have a single degree of freedom (DOF) representing the torsion coordinate. The system in total has 17 nodes and accordingly a total of 92 coordinates.

The stiffness and mass matrices of each beam element are determined and assembled to form the stiffness $[K_{sp}]$ and mass $[M_{sp}]$ matrices of the pinion shaft, and stiffness $[K_{sg}]$ and mass $[M_{sg}]$ matrices of gear shaft. Overall shaft stiffness and mass matrices of the system are then assembled via superposition according to the following process given by and $[K_s] = Diag[[K_{sp}]\ldots[K_{sg}]\ldots]$ and $[M_s] = Diag[[M_{sp}]\ldots [M_{sg}]\ldots]$.

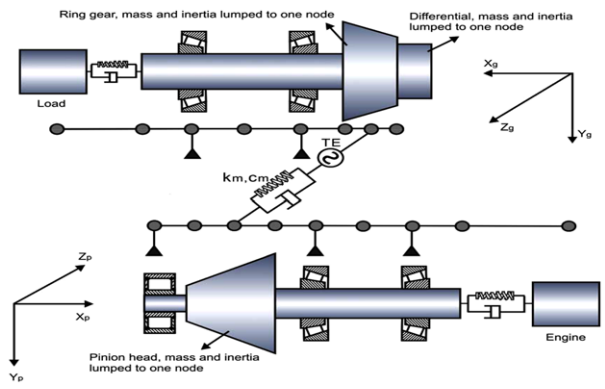

Figure 1. Schematic of the setup for the dynamic finite element modeling of a spiral bevel geared rotor system.

The engine and load are separately connected to one node at the pinion shaft, and one node at the gear shaft, respectively, with torsional springs. The stiffness matrices of the torsional spring elements used to connect the engine and pinion shaft, and the load and gear shaft can be written in terms of individual torsional spring stiffness as $[K_{tsp}]$ and $[K_{tsg}]$; both of which are 7x7 square matrices. The overall stiffness matrices of torsional spring elements of the whole system can be written as $[K_{ts}] = Diag[\ldots[K_{tsp}]\ldots[K_{tsg}]]$. The overall mass matrices of the engine and load of the complete system can be written in terms of torsional moment of inertia of engine I_E and load I_L as $[M_{E,L}] = Diag[\ldots I_E \ldots I_L]$.

In practical applications, the pinion shaft is usually supported by 2 or 3 bearings and gear shaft is usually supported by only 2 bearings. For a system having a total of n bearings, the overall bearing stiffness matrix of the complete system can be written by assembling the individual bearing element stiffness matrices $[K_{bi}]$(i=1 to n) as $[K_b] = [\ldots[K_{b1}]\ldots[K_{b2}]\ldots[K_{b3}]\ldots[K_{bn}]\ldots]$.

The gear stiffness coupling matrix for the mesh coupling between the two nodes representing the pinion head and ring gear is derived from the free vibration equation of motion of the spiral bevel gear pair. The dynamic model of the spiral bevel gear pair is shown in Figure 2. The pinion and gear, which are modeled as rigid bodies, are connected by a linear set of gear mesh spring and damper elements. Using the quasi-static three-dimensional finite element tooth contact analysis program (Vijayakar, 1991, 2003) and the concept of contact cells (Cheng, 2000), the averaged mesh point, averaged line-of-action, averaged mesh stiffness and loaded transmission error are obtained for use to construct the mesh spring connecting point, mesh spring direction, mesh spring stiffness and transmission error excitation between the pinion and gear. Both pinion and gear are allowed to move in 6 directions such that the gear pair dynamic system in total has 12 degrees of freedom. The generalized coordinates of pinion and gear are separately expressed as $\{q_{pg}\} = \{x_p, y_p, z_p, \theta_{px}, \theta_{py}, \theta_{pz}, x_g, y_g, z_g, \theta_{gx}, \theta_{gy}, \theta_{gz}\}^T$. Hence, the undamped free vibration equations for this gear pair dynamic system can be expressed as:

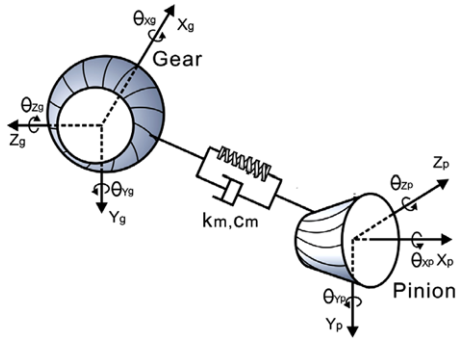

Figure 2. Spiral bevel gear pair dynamic model.

$$m_p\ddot{x}_p - k_m pn_{px} = 0$$
$$m_p\ddot{y}_p - k_m pn_{py} = 0 \quad (1a,b,c)$$
$$m_p\ddot{z}_p - k_m pn_{pz} = 0$$

$$I_{px}\ddot{\theta}_{px} - k_m pn_{pz}y_{pm} + k_m pn_{py}z_{pm} = 0$$
$$I_{py}\ddot{\theta}_{py} - k_m pn_{px}z_{pm} + k_m pn_{pz}x_{pm} = 0 \quad (2a,b,c)$$
$$I_{pz}\ddot{\theta}_{pz} - k_m pn_{py}x_{pm} + k_m pn_{px}y_{pm} = 0$$

$$m_g\ddot{x}_g + k_m pn_{gx} = 0$$
$$m_g\ddot{y}_g + k_m pn_{gy} = 0 \quad (3a,b,c)$$
$$m_g\ddot{z}_g + k_m pn_{gz} = 0$$

$$I_{gx}\ddot{\theta}_{gx} + k_m pn_{gz}y_{gm} - k_m pn_{gy}z_{gm} = 0$$
$$I_{gy}\ddot{\theta}_{gy} + k_m pn_{gx}z_{gm} - k_m pn_{gz}x_{gm} = 0 \quad (4a,b,c)$$
$$I_{gz}\ddot{\theta}_{gz} + k_m pn_{gy}x_{gm} - k_m pn_{gx}y_{gm} = 0$$

where, (n_{lx}, n_{ly}, n_{lz}) is the line-of-action vector, (n_{lm}, n_{lm}, n_{lm}) ($l = p$, g) is the mesh point vector. $l = p$, g refers to the pinion and gear local coordinate systems, respectively. Here, k_m is mesh stiffness. p is relative displacement between pinion and gear along line-of-action and is expressed as:

$$\begin{aligned} p = {} & x_g n_{gx} + y_g n_{gy} + z_g n_{gz} + \theta_{gx} y_{gm} n_{gz} - \theta_{gx} z_{gm} n_{gy} + \theta_{gy} z_{gm} n_{gx} - \theta_{gy} x_{gm} n_{gz} \\ & + \theta_{gz} x_{gm} n_{gy} - \theta_{gz} y_{gm} n_{gx} - x_p n_{px} - y_p n_{py} - z_p n_{pz} - \theta_{px} y_{pm} n_{pz} + \theta_{px} z_{pm} n_{py} \\ & - \theta_{py} z_{pm} n_{px} + \theta_{py} x_{pm} n_{pz} - \theta_{pz} x_{pm} n_{py} + \theta_{pz} y_{pm} n_{px} \end{aligned} \quad (5)$$

By combining equations (1) ~ (5), a clearer equation of motion can be obtained as:

$$[m_{pq}]\{\ddot{q}_{pq}\} + [k_{pg}]\{q_{pg}\} = 0 \quad (6)$$

$$[m_{pg}] = diag[m_p, m_p, m_p, I_{px}, I_{py}, I_{pz}, m_g, m_g, m_g, I_{gx}, I_{gy}, I_{gz}] \quad (7)$$

$$[k_{pg}] = \begin{bmatrix} k_m\{h_p\}^T\{h_p\} & -k_m\{h_p\}^T\{h_g\} \\ -k_m\{h_g\}^T\{h_p\} & k_m\{h_g\}^T\{h_g\} \end{bmatrix} \quad (8)$$

In the above equations, $\{h_p\}$ and $\{h_g\}$ are the coordinate transformation vectors between the spiral bevel gear line-of-action direction and generalized coordinate directions for pinion and gear separately. They are expressed as:

$$\{h_l\} = \{n_{lx}, n_{ly}, n_{lz}, \lambda_{lx}, \lambda_{ly}, \lambda_{lz}\}(l = p, g) \quad (9)$$

$$\{\lambda_{lx}, \lambda_{ly}, \lambda_{lz}\} = \{y_l n_{lz} - z_l n_{ly}, z_l n_{lx} - x_l n_{lz}, x_l n_{ly} - y_l n_{lx}\}(l = p, g) \quad (10)$$

The gear mesh stiffness matrix $[k_{pg}]$ and the mass matrix $[m_{pg}]$ of the gear pair can be obtained from equations (6) ~ (10). The overall gear mesh stiffness and mass matrices of the whole system can then be obtained from $[k_{pg}]$ = *Diag*[…$[k_{pg}]$…] and $[M_{pg}]$ = *Diag*[…$[m_{pg}]$…].

Accordingly, the mass and stiffness matrices of the whole dynamic finite element model are derived as $[M] = [M_{pg}]+[M_s]+[M_{E,L}]$, $[K] = [K_{pg}]+[K_s]+[K_b]+[K_{ts}]$. Also, the system proportional damping matrix $[C]$ used in this model and the expression of the overall system excitation vector $\{F(t)\}$ is given as:

$$[C] = \zeta_s([K_s] + [K_b] + [K_{ts}]) + \zeta_m[K_{pg}] \quad (11)$$

$$\{F(t)\} = [\cdots\{h_p\}\cdots - \{h_g\}\cdots]^T(k_m + c_m j)e(t) \quad (12)$$

where ζ_s is the system damping ratio, and ζ_m is the mesh damping ratio.

The equation of motion of the whole spiral bevel geared rotor system can be expressed as:

$$[M]\{\ddot{X}(t)\} + [C]\{\dot{X}(t)\} + [K]\{X(t)\} = \{F(t)\} \quad (13)$$

The direct matrix inversion method is applied here to calculate the steady state forced response as:

$$\{X(t)\} = [H(\omega)]^{-1}\{F(t)\} \quad (14)$$

The dynamic responses of the pinion head $\{X_p\}$ and ring gear $\{X_g\}$ can then be extracted from $X(t)$ to calculate the dynamic transmission error given by the following equation:

$$\delta_d = \{h_p\}\{X_p\} - \{h_g\}\{X_g\}. \quad (15)$$

The dynamic mesh force along the line-of-action is expressed as:

$$F_m = k_m(\delta_d - \varepsilon_0) + c_m(\dot{\delta}_d - \dot{\varepsilon}_0) \quad (16)$$

where, k_m is the mesh stiffness, $c_m = \zeta_m k_m$ is the mesh damping, and ε_0 is the loaded transmission error.

It may be noted that, in the present study, the spiral bevel geared rotor system as shown in Figure 1 is used to apply the proposed dynamic finite element modeling theory. However, the same theory can be applied to spiral bevel geared rotor systems with other kinds of pinion and gear configurations.

3. ENHANCED LUMPED PARAMETERS

3.1. Spiral Bevel Gear Model

A 14-DOF lumped parameter dynamic model (Cheng, 2000) representing a spiral bevel gear train assembly used in this study comprises of a spiral bevel gear pair, an engine element and a load element as illustrated in Figure 3. Both engine and load have a single DOF in the torsional direction. The pinion and gear are both modeled as rigid bodies having 6 Cartersian coordinates. The torsional springs are used to connect the pinion and engine as well as to attach gear and load. The meshing between the pinion

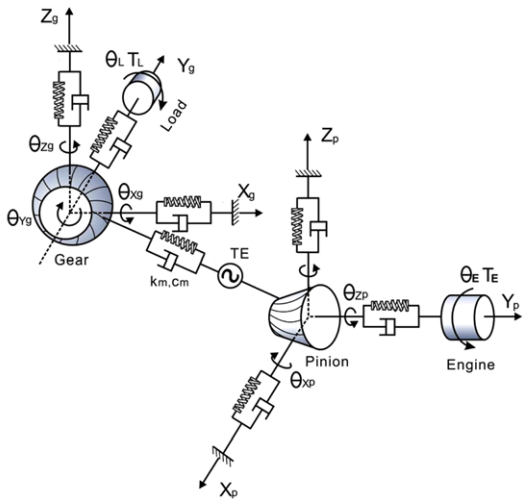

Figure 3. Spiral bevel geared rotor systems represented by a 14-DOF lumped parameter dynamic model.

and gear is represented with a mesh coupling. The averaged mesh stiffness is given by k_m, and the static transmission error is denoted by *TE*. Since the pinion and gear are modeled as rigid bodies, their mass and inertia effects are lumped at their centroid points. The lumped shaft-bearing springs are connected to each lumped point of the pinion and gear to act as the support for the gearing assembly. Given these assumption, the equations of motion in matrix form can be easily derived and expressed as:

$$[M]\{\ddot{q}\}+[C]\{\dot{q}\}+[K]\{q\}=\{F(t)\} \tag{17}$$

where the generalized coordinates are given by:

$$\{q\}=\{\theta_E,\{q_p\}^T,\{q_g\}^T,\theta_L\}^T \tag{18}$$

$$\{q_l\}=\{x_l,y_l,z_l,\theta_{lx},\theta_{ly},\theta_{lz}\}^T \quad (l=p,\ g) \tag{19}$$

The lumped mass and stiffness matrices are described as:

$$[M]=diag[I_E,M_{px},M_{py},M_{pz},I_{px},I_{py},I_{pz},M_{gx},M_{gy},M_{gz},I_{gx},I_{gy},I_{gz},I_L] \tag{20}$$

$$[K]=Diag[\cdots[K_{ll}]\cdots]+Diag[\cdots[K_{pg}]\cdots]+Diag[[K_{tsp}]\cdots[K_{tsg}]] \tag{21}$$

In the above equation, $[K_{ll}]$ is the lumped shaft-bearing stiffness matrix, $[K_{pg}]$ is the gear mesh coupling stiffness matrix, $[K_{tsp}]$ is the coupling stiffness matrix of the torsional spring used to connect pinion and engine, and $[K_{tsg}]$ is the coupling stiffness matrix of the torsional spring used to connect gear and load. The damping [C] is assumed to be system proportional that is expressed as:

$$[C]=\zeta_s(Diag[\cdots[K_{ll}]\cdots]+Diag[[K_{tsp}]\cdots[K_{tsg}]])+\zeta_m Diag[\cdots[K_{pg}]\cdots] \tag{22}$$

where ζ_s is system damping ratio and ζ_m is mesh damping ratio. The force vector $\{F(t)\}$ at the right side of equation (17) is,

$$\{F(t)\}=[\cdots\{h_p\},-\{h_g\}\cdots]^T(k_m+c_m j)e(t) \tag{23}$$

Here, $\{h_p\}$ and $\{h_g\}$ are the coordinate transformation vectors between the spiral bevel gear line-of-action direction and generalized coordinate directions for pinion and gear separately. They are explicitly expressed as,

$$\{h_l\}=\{n_{lx},n_{ly},n_{lz},\lambda_{lx},\lambda_{ly},\lambda_{lz}\} \tag{24}$$

$$\{\lambda_{lx},\lambda_{ly},\lambda_{lz}\}=\{y_l n_{lz}-z_l n_{ly},z_l n_{lx}-x_l n_{lz},x_l n_{ly}-y_l n_{lx}\} \tag{25}$$

where $\{n_{lx},\ n_{ly},\ n_{lz}\}$ is the line-of-action vector; $\{x_l,\ y_l,\ z_l\}$ is the mesh point vector; and $l = p, g$ refers to pinion and gear local coordinate systems respectively.

The dynamic transmission error δ_d is calculated in frequency domain and expressed as,

$$\delta_d=h_p\{q_p\}-h_g\{q_g\} \tag{26}$$

The corresponding dynamic mesh force along line-of-action direction is expressed as:

$$F_m=k_m(\delta_d-\varepsilon_0)+c_m(\dot{\delta}_d-\dot{\varepsilon}_0) \tag{27}$$

where k_m is mesh stiffness, $c_m = \zeta_s k_m$ is mesh damping, and ε_0 is loaded transmission error.

The most critical deficiency of this model lies in the fact that it is a lack of a fully validated method to synthesize the lumped point parameters, that is the lumped shaft-bearing stiffness matrix $[K_{ll}]$, and lumped mass and inertia elements of the pinion M_{px}, M_{py}, M_{pz}, I_{px}, I_{py}, I_{pz} and gear M_{gx}, M_{gy}, M_{gz}, I_{gx}, I_{gy}, I_{gz}, which are key to representing shaft-bearing structural dynamic characteristics. The lack of a more comprehensive representation may cause inaccuracy in the predicted dynamic response, especially if the lumped point parameters are not well determined.

3.2. New Lumped Parameter Formulation

The basic idea of proposed lumped parameter synthesis theory is to approximate the continuous parameter models of the pinion and gear in lumped parameter models, while being able to retain the same first order pinion and gear-shaft bending modes. The fundamental formulation is given below. First, the shaft-bearing stiffness model is described and then followed by the derivation for mass and inertia elements.

3.2.1. Shaft-bearing stiffness

In this section, the equivalent shaft-bearing stiffness relative to the lumped point is formulated applying a static finite element model. The analysis is performed on a 3-

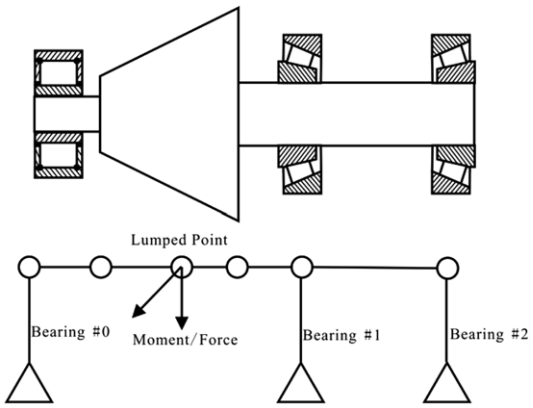

Figure 4. Finite element modeling of 3-bearing straddle mounted pinion configuration .

bearing straddle mounted pinion configuration as shown in Figure 4. The pinion with integrated shaft is modeled with several uniform cross-section beam elements, while the support bearings are modeled using a stiffness matrix based on an earlier formulation developed by Lim *et al*. (Lim and Singh 1990a, 1990b, 1990c; Liew and Lim, 2005).

For a unit load at the lumped point, the static equilibrium equation applying the finite element theory can be expressed as:

$$\{P\}+\{R\}=[S]\{\Delta\} \tag{28}$$

where *{P}* represents the external load exerted at all the nodes, *{R}* represents the reaction load at all the nodes, [*S*] is the assembled stiffness matrix, and {*Δ*} represents the displacements of all the nodes. A more detailed equation can be derived from equation (28) as:

$$\begin{Bmatrix} P^F \\ P^S \end{Bmatrix}+\begin{Bmatrix} R^F \\ R^S \end{Bmatrix}=\begin{bmatrix} S^{FF} & S^{FS} \\ S^{SF} & S^{SS} \end{bmatrix}\begin{Bmatrix} \Delta^F \\ \Delta^S \end{Bmatrix} \tag{29}$$

where P^j and R^j refer to the external and reaction loads, respectively, exerted at the nodes of the part of pinion with the integrated shaft ($j=F$) and bearing outer raceway ($j=S$), and the symbol Δ^j represents the nodal displacements of the pinion-shaft ($j=F$) and bearing outer raceway ($j=S$).

Since the reaction load is only exerted at the nodes at the bearing outer races and the nodes at the bearing outer races are fixed, R^F and Δ^s in equation (29) can be set to be zero yielding,

$$\begin{Bmatrix} P^F \\ P^S \end{Bmatrix}+\begin{Bmatrix} 0 \\ R^S \end{Bmatrix}=\begin{bmatrix} S^{FF} & S^{FS} \\ S^{SF} & S^{SS} \end{bmatrix}\begin{Bmatrix} \Delta^F \\ 0 \end{Bmatrix} \tag{30}$$

Thus, the following expression can be drawn from the above equation (30):

$$\{\Delta^F\}=[S^{FF}]^{-1}\{P^F\} \tag{31}$$

In the above equation, the lumped point displacement $\{\Delta_1^l\}$ can be obtained from $\{\Delta^F\}$. The relationship among the unit external load at the lumped point $\{P_1^l\}$, the displacement of the lumped point $\{\Delta_1^l\}$ and the equivalent shaft-bearing stiffness relative to the lumped point $[K^{ll}]$ can be expressed as:

$$\{P_1^l\}=[K^{ll}]\{\Delta_1^l\} \tag{32}$$

Repeating the above procedure, by adding a unit load in the other five nodal coordinates individually one at a time, the lumped point displacements corresponding to each unit load can be constructed as $\{\Delta_i^l\}$ (i =2,3,4,5,6). The unit load at the lumped point in each of other 5 directions can also similarly be written as $\{P_1^l\}$ (i =2,3,4,5,6). Accordingly, the following relationship could be obtained:

$$\{P_i^l\}=[K^{ll}]\{\Delta_i^l\}(i=2,3,4,5,6) \tag{33}$$

Combining equations (32) and (33) yield,

$$[P_1^l \;\; P_2^l \;\; P_3^l \;\; P_4^l \;\; P_5^l \;\; P_6^l]=[K^{ll}][\Delta_1^l \;\; \Delta_2^l \;\; \Delta_3^l \;\; \Delta_4^l \;\; \Delta_5^l \;\; \Delta_6^l] \tag{34}$$

Hence, the equivalent shaft-bearing stiffness relative to the lumped point $[K^{ll}]$ can be calculated as:

$$[K^{ll}]=[P_1^l \;\; P_2^l \;\; P_3^l \;\; P_4^l \;\; P_5^l \;\; P_6^l][\Delta_1^l \;\; \Delta_2^l \;\; \Delta_3^l \;\; \Delta_4^l \;\; \Delta_5^l \;\; \Delta_6^l]^{-1} \tag{35}$$

However, the equivalent shaft-bearing stiffness calculated from the finite element equilibrium model may not accurately describe the equivalent axial translational stiffness. Therefore, the axial translational stiffness model of the 3-bearing straddle mounted pinion configuration shown in Figure 5 has to be separately formulated in order to refine the axial translational stiffness described by equivalent shaft-bearing stiffness $[K^{ll}]$. In Figure 5, K_{b1} and K_{b2} are axial translational stiffnesses of bearings 1 and 2. Note that K_{s1} is the shaft axial stiffness from the load point to the center of bearing 1, and similarly, K_{s2} is shaft axial stiffness from the center of bearing 1 to the center of bearing 2. Also, K_c is additional cascade stiffness associated with bearing 2 to represent the shaft-bolt-york elasticity between the center and inner race of bearing 2. The housing bolt stiffness is given by K_{hb}.

The axial translation stiffness of $[K^{ll}]$ calculated from the finite element representation does not take K_c and K_{hb} into account. Hence, a refinement can be performed according to Figure 5 in the following way. Before applying the finite element calculation, the cascade stiffness K_{s3} should be added into the axial translation stiffness of bearing 2 $K_{b2.}$ After performing the finite element modeling, the

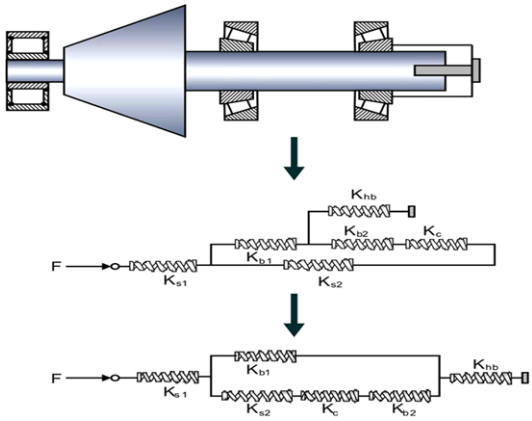

Figure 5. Axial translational stiffness model.

temporary equivalent shaft-bearing stiffness can then be obtained. Finally, the temporary equivalent shaft-bearing stiffness can be use to add K_{hb} into its axial translation stiffness to obtain the eventual equivalent lumped shaft-bearing stiffness of the 3-bearing straddle mounted pinion.

Even though the above analysis is applied to the 3-bearing configuration, the approach of computing the equivalent lumped shaft-bearing stiffness of other pinion and gear configurations (Peng and Lim, 2007c) can be calculated in the similar way.

3.2.2. Lumped mass and inertia

The first bending mode shape functions of integrated pinion-shaft and gear–shaft assemblies are first generated using the Initial Parameter Method described in Reference (Karnovsky, 2003). In this paper, to calculate first bending mode shape function, the coordinate system as shown in Figure 6 is used. The Initial Parameter Method is generally applied to perform dynamical calculations of beams with arbitrary peculiarities and varying types of boundary conditions.

In Figure 6, the dotted line at y=0 to the left represents an arbitrary type of support. Transverse displacement z_0, angle of rotation φ_0, bending moment M_0 and shear force Q_0 at y=0 are called initial parameters. State parameters transverse displacement z(y), angle of rotation $\varphi(y)$, bending moment $M(y)$, shear force $Q(y)$ at any position x may be presented in the following forms (Karnovsky, 2003):

$$z(y) = z_0 S(ky) + \varphi_0 \frac{T(ky)}{k} + M_0 \frac{U(ky)}{k^2 EI} + Q_0 \frac{V(ky)}{k^3 EI} + \frac{1}{k^2 EI}\left(\frac{1}{k}\sum R_i V[k(y-y_i)] + \frac{\omega^2}{k}\sum M_i z_i V[k(y-y_i)] - \omega^2 \sum J_i \varphi_i U[k(y-y_i)]\right) \quad (36)$$

$$\varphi(y) = z_0 V(ky)k + \varphi_0 S(ky) + M_0 \frac{T(ky)}{kEI} + Q_0 \frac{U(ky)}{k^2 EI} + \frac{1}{kEI}\left(\frac{1}{k}\sum R_i U[k(y-y_i)] + \frac{\omega^2}{k}\sum M_i z_i U[k(y-y_i)] - \omega^2 \sum J_i \varphi_i T[k(y-y_i)]\right) \quad (37)$$

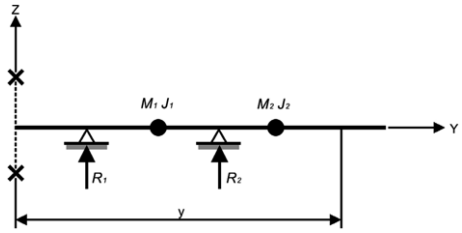

Figure 6. Design of beam with lumped mass points.

$$M(y) = z_0 U(ky) EIk^2 + \varphi_0 V(ky) EIk + M_0 S(ky) + Q_0 \frac{T(ky)}{k} + \frac{1}{k}\sum R_i U[k(y-y_i)] + \frac{\omega^2}{k}\sum M_i z_i T[k(y-y_i)] - \omega^2 \sum J_i \varphi_i S[k(y-y_i)] \quad (38)$$

$$Q(y) = z_0 T(ky) EIk^3 + \varphi_0 U(ky) EIk^2 + M_0 V(ky)k + Q_0 S(ky) + \sum R_i S[k(y-y_i)] + \omega^2 \sum M_i z_i S[k(y-y_i)] - \omega^2 k \sum J_i \varphi_i V[k(y-y_i)] \quad (39)$$

where M_i is the i[th] lumped mass (note: M_0 = bending moment at x=0), J_i is the moment of inertia of the i[th] lumped mass, R_i is the i[th] concentrated force (active or reactive), y_i is distance between origin and point of application R_i or M_i,z_i, and φ_i are the vertical displacement and slope, respectively, where the lumped mass M_i is located, and $S(y)$, $T(y)$, $U(y)$ and $V(y)$ are Krylov-Duncan functions given as:

$$S(ky) = \frac{1}{2}(\cosh ky + \cos ky)$$
$$T(ky) = \frac{1}{2}(\sinh ky + \sin ky)$$
$$U(ky) = \frac{1}{2}(\cosh ky - \cos ky) \quad (40a,b,c,d)$$
$$V(ky) = \frac{1}{2}(\sinh ky - \sin ky)$$

where, $k=\sqrt[4]{\frac{m}{EI}\omega^2}$ is the frequency parameter, m is the linear density of the uniform beam, ω is radian natural frequency, E is the Young's modulus of elasticity, and I is the rotary inertia of the cross-sectional area of the beam.

This theory can generally be applied to the pinion and

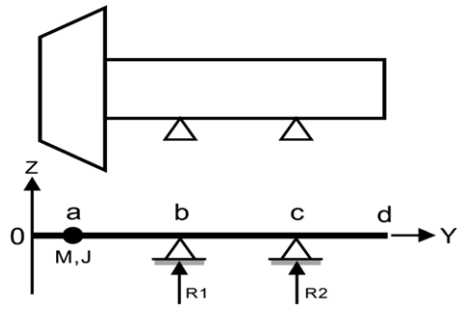

Figure 7. Beam with lumped mass representation of the pinion with integrated shaft.

gear sets in the spiral bevel geared rotor system. Consider an overhung mounted and simply supported pinion example as shown in Figure 7. The pinion is modeled as a uniform beam with a lumped mass at the lumped point **a**. Accordingly, the transverse displacement z(y), angle of rotation, bending moment $\varphi(y)$, shear force at any position y of the pinion model shown in Figure 7 can be expressed by using the Initial Parameter Method (Karnovsky, 2003) as:

$$z(y) = z_0 S(ky) + \varphi_0 \frac{T(ky)}{k} + M_0 \frac{U(ky)}{k^2 EI} + Q_0 \frac{V(ky)}{k^3 EI} + \frac{1}{k^2 EI}\left(\frac{1}{k} R_1 V[k(y-b)] + \frac{1}{k} R_2 V[k(y-c)]\right) + \frac{1}{k^2 EI}\left(\frac{\omega^2}{k} Mz(a) V[k(y-a)] - \omega^2 J\varphi(a) U[k(y-a)]\right) \quad (41)$$

$$\varphi(y) = z_0 V(ky)k + \varphi_0 S(ky) + M_0 \frac{T(ky)}{kEI} + Q_0 \frac{U(ky)}{k^2 EI} + \frac{1}{kEI}\left(\frac{1}{k} R_1 U[k(y-b)] + \frac{1}{k} R_2 U[k(y-c)]\right) + \frac{1}{kEI}\left(\frac{\omega^2}{k} Mz(a) U[k(y-a)] - \omega^2 J\varphi(a) T[k(y-a)]\right) \quad (42)$$

$$M(y) = z_0 U(ky) EIk^2 + \varphi_0 V(ky) EIk + M_0 S(ky) + Q_0 \frac{T(ky)}{k} + \frac{1}{k} R_1 U[k(y-b)] + \frac{1}{k} R_2 U[k(y-c)] + \frac{\omega^2}{k} Mz(a) T[k(y-a)] - \omega^2 J\varphi(a) S[k(y-a)] \quad (43)$$

$$Q(y) = z_0 T(ky) EIk^3 + \varphi_0 U(ky) EIk^2 + M_0 V(ky)k + Q_0 S(ky) + R_1 S[k(y-b)] + R_2 S[k(y-c)] + \omega^2 Mz(a) S[k(y-a)] - \omega^2 kJ\varphi(a) V[k(y-a)] \quad (44)$$

The boundary condition can be described mathematically as $M_0 = 0; Q_0 = 0; z(b) = 0; z(c) = 0; M(d) = 0; Q(d) = 0$. By applying these boundary conditions to equations (41) ~ (44), the following set of equations can be obtained:

$$z(b) = z_0 S(kb) + \varphi_0 \frac{T(kb)}{k} + \frac{1}{k^2 EI}\left(\frac{\omega^2}{k} M z(a) V[k(b-a)] - \omega^2 J\varphi(a) U[k(b-a)]\right) = 0 \quad (45)$$

$$z(c) = z_0 S(kc) + \varphi_0 \frac{T(kc)}{k} + \frac{1}{k^2 EI}\left(\frac{1}{k} R_1 V[k(c-b)] + \frac{\omega^2}{k} M z(a) V[k(c-a)] - \omega^2 J\varphi(a) U[k(c-a)]\right) = 0 \quad (46)$$

$$M(d) = z_0 EIk^2 U(kd) + \varphi_0 EIkV(kd) + \frac{1}{k} R_1 T[k(d-b)] + \frac{1}{k} R_2 T[k(d-c)] + \frac{\omega^2}{k} M z(a) T[k(d-a)] - \omega^2 J\varphi(a) S[k(d-a)] = 0 \quad (47)$$

$$Q(d) = z_0 EIk^3 T(kd) + \varphi_0 EIk^2 U(kd) + R_1 S[k(d-b)] + R_2 S[k(d-c)] + \omega^2 M z(a) S[k(d-a)] - \omega^2 kJ\varphi(a) V[k(d-a)] = 0 \quad (48)$$

The displacement and angle of rotation at $y=a$ are expressed as:

$$z(a) = z_0 S(ka) + \varphi_0 \frac{T(ka)}{k} \quad (49)$$

$$\varphi(a) = z_0 V(ka)k + \varphi_0 S(ka) \quad (50)$$

Therefore, the system of homogeneous equations can be obtained. If and only if the following determinant, which represents the frequency domain, is zero, the system has a non-trivial solution.

$$\left| [r_1 \quad r_2 \quad r_3 \quad r_4]^T \right| = 0 \quad (51)$$

$$r_1 = \begin{Bmatrix} S(kb) + \frac{\omega^2}{k^3 EI} MV[k(b-a)] S(ka) - \frac{\omega^2}{kEI} JU[k(b-a)] V(ka) \\ \frac{T(kb)}{k} + \frac{\omega^2}{k^4 EI} MV[k(b-a)] T(ka) - \frac{\omega^2}{k^2 EI} JU[k(b-a)] S(ka) \\ 0 \\ 0 \end{Bmatrix}^T \quad (52)$$

$$r_2 = \begin{Bmatrix} S(kc) + \frac{\omega^2}{k^3 EI} MV[k(c-a)] S(ka) - \frac{\omega^2}{kEI} JU[k(c-a)] V(ka) \\ \frac{T(kc)}{k} + \frac{\omega^2}{k^4 EI} MV[k(c-a)] T(ka) - \frac{\omega^2}{k^2 EI} JU[k(c-a)] S(ka) \\ \frac{V[k(c-b)]}{k^3 EI} \\ 0 \end{Bmatrix}^T \quad (53)$$

$$r_3 = \begin{Bmatrix} EIk^2 U(kd) + \frac{\omega^2 MT[k(d-a)] S(ka)}{k} - \omega^2 JS[k(d-a)] V(ka) \\ EIkV(kd) + \frac{\omega^2 M}{k^2} T[k(d-a)] T(ka) - \omega^2 JS[k(d-a)] S(ka) \\ \frac{1}{k} T[k(d-b)] \\ \frac{1}{k} T[k(d-c)] \end{Bmatrix}^T \quad (54)$$

$$r_4 = \begin{Bmatrix} EIk^3 T(kd) + \omega^2 MS[k(d-a)] S(ka) - \omega^2 k^2 JV[k(d-a)] V(ka) \\ EIk^2 U(kd) + \frac{\omega^2 MS[k(d-a)] T(ka)}{k} - \omega^2 kJV[k(d-a)] S(ka) \\ S[k(d-b)] \\ S[k(d-c)] \end{Bmatrix}^T \quad (55)$$

In the above problem, multiple solutions of k that are expressed as k_1, k_2, k_3, k_4, k_5 can be obtained. Here, k_1, is the smallest value of k, which is for the first bending mode. Substitution of the value of k_1 into the above equation and rearranging yields z_0, R_1, R_2, in terms of φ_0. Then, further substitution of the relationship into equations (41), (42) can

produce the mode shape functions z(y), $\varphi(y)$.

Then, according to the balance of kinetic energy at the first bending mode, the first equation could be expressed as:

$$\int_0^l 0.5 \cdot m(y) z^2(y)\, dy + 0.5M \cdot z^2(a) + 0.5J \cdot \varphi^2(a) = 0.5 \cdot M_{effective} z^2(a) + 0.5 I_{effective} \varphi^2(a) \quad (56)$$

where, $M_{effective}$ and $I_{effective}$ are the pinion's effective mass and effective moment of inertia that need to be determined.

As for the model in Figure 7, the lumped stiffness relative to Point **a** and the first bending natural frequency can be obtained as $[K_a]_{2\times2}$ and ω_1. As the continuous parameter model in Figure 7 and its equivalent 2-DOF lumped parameter model should have the same first bending natural frequency ω_1. The second equation could be expressed according to ω_1 as:

$$\left| [K_a] - \omega_1^2 \begin{bmatrix} M_{effective} & 0 \\ 0 & I_{effective} \end{bmatrix} \right| = 0 \quad (57)$$

Using equations (56) and (57), the effective mass $M_{effective}$ and effective moment of inertia $I_{effective}$ can then be obtained. Then, in equation (20), the lumped mass and inertia of pinion can be expressed as:

$$M_{px} = M_{pz} = M_{effective},\ I_{px} = I_{pz} = I_{effective} \quad (58)$$

$$M_{py} = M_{total},\ I_{py} = J_{torsion} \quad (59)$$

where, M_{total} is the total mass of pinion, and $J_{torsion}$ is the torsional moment of inertia of pinion. Note that x is in horizontal direction, y is in axial direction, and z is in vertical direction.

It may be noted that M_{total}, $J_{torsion}$ are directly used for M_{py}, I_{py} since the pinion does not have torsional and axial translational deformations when the geared rotor system is excited at relatively low frequency. Also, the lumped mass and inertia elements of the pinion or gear with other kinds of configurations can be calculated by following the procedure outlined above. For brevity, the detail presentations are not given here.

4. COMPARATIVE ANALYSIS AND DISCUSSIONS

Using the dynamic finite element model and the previous lumped parameter approach, the dynamic mesh force is calculated and plotted in Figures 8-10 for the following three pinion-gear configurations: (a) pinion and gear are both overhung mounted and simply supported, (b) pinion and gear are both overhung mounted and flexibly supported, and (c) pinion is straddle mounted and flexibly supported

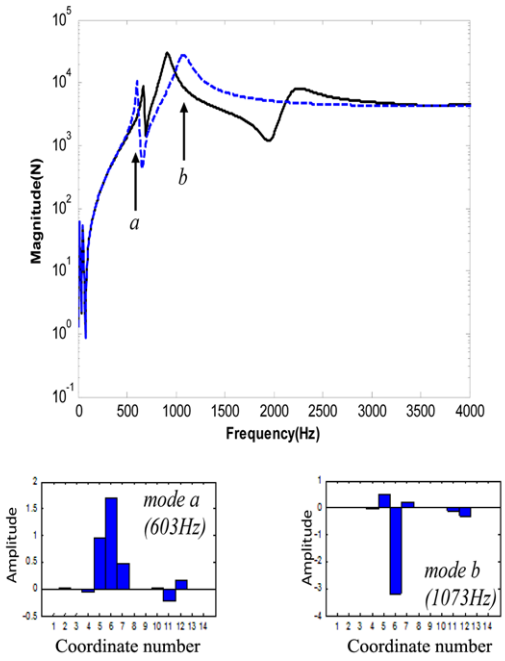

Coordinate Number	1	2	3	4	5	6	7	8	9	10	11	12	13	14
DOF	θ_E	X_p	Y_p	Z_p	θ_{xp}	θ_{yp}	θ_{zp}	X_g	Y_g	Z_g	θ_{xg}	θ_{yg}	θ_{zg}	θ_L

Figure 8. Comparison of the predicted dynamic mesh forces applying the dynamic finite element model (solid line——) and previous basic lumped parameter model (dashed dotted line------) for case (a) with pinion and gear both overhung mounted and simply supported.

while gear is overhung mounted and flexibly supported.

Predicted results reveal that the dynamic mesh forces obtained from the two models are different at some of the structural modes. Figure 8 shows that the dynamic responses do not match at modes *a* and *b*. By examining the corresponding mode shapes in the basic lumped parameter model, it is found that the contributions of coordinate numbers 5 and 7, representing pinion bending, to the mode shapes are significant. Similar behavior is observed in Figure 9 where modes *a*, *b*, *c* of the previous basic lumped parameter model fail to match with the dynamic finite element dynamic model. Coordinate numbers 5 and 7 also show major contributions to these three mode shapes. In Figure 10, however, mode *a* of the previous lumped parameter model matches very well with proposed finite element model, while modes *b* and *c* depict some discrepancies. It is observed from the mode shapes that mode *a* is not coupled to the pinion bending response represented by coordinate numbers 5 and 7 or to the gear bending represented by coordinate numbers 11 and 13 unlike modes *b* and *c*, which are coupled to the critical pinion bending and gear bending responses. In fact, the results in Figures 8-10 indicate that dynamic responses of dynamic finite element model and basic lumped parameter

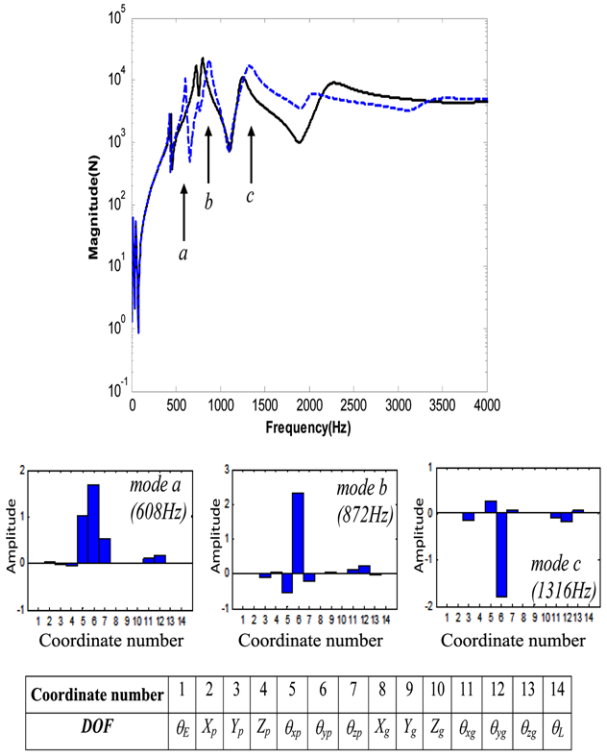

Coordinate number	1	2	3	4	5	6	7	8	9	10	11	12	13	14
DOF	θ_E	X_p	Y_p	Z_p	θ_{xp}	θ_{yp}	θ_{zp}	X_g	Y_g	Z_g	θ_{xg}	θ_{yg}	θ_{zg}	θ_L

Figure 9. Comparison of the predicted dynamic mesh forces applying the dynamic finite element model (solid line ——) and previous basic lumped parameter model (dashed dotted line -------) for case (b) with pinion and gear both overhung mounted and flexibly supported.

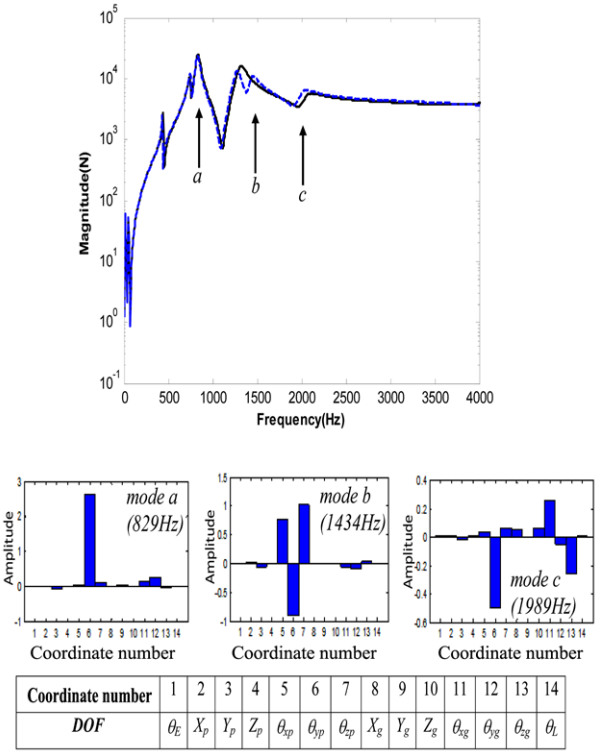

Coordinate number	1	2	3	4	5	6	7	8	9	10	11	12	13	14
DOF	θ_E	X_p	Y_p	Z_p	θ_{xp}	θ_{yp}	θ_{zp}	X_g	Y_g	Z_g	θ_{xg}	θ_{yg}	θ_{zg}	θ_L

Figure 10. Comparison of the predicted dynamic mesh forces applying the dynamic finite element model (solid line ——) and previous basic lumped parameter model (dashed dotted line -------) for case (c) with pinion straddle mounted, gear overhung mounted and both flexibly supported.

model do not match well at the modes that are coupled to pinion or gear bending responses.

When compared to the dynamic finite element solution, the mesh force calculated using the proposed, newly enhanced lumped parameter model shows good agreement especially at the low frequency range where a perfect match is observed, as shown in Figures 11-13 for the three configurations described above. Results show that the proposed lumped parameter model has the potential to accurately calculate the dynamic mesh force as compared to the previous one.

Unlike the previous lumped parameter model, where the total value of mass and inertia elements is used in the lumped parameter synthesis method, the newly proposed lumped parameter model lumps only the effective mass and inertia elements. The use of effective mass and inertia elements leads to more accurate representation of system mass matrix to improve the accuracy of the shaft-bearing dynamic characteristics. This yields more accurate modal responses, especially when the contribution of bending modes is significant.

It has to be noted though, at the high frequency range, the dynamic finite element model and proposed lumped parameter model results still show some minor

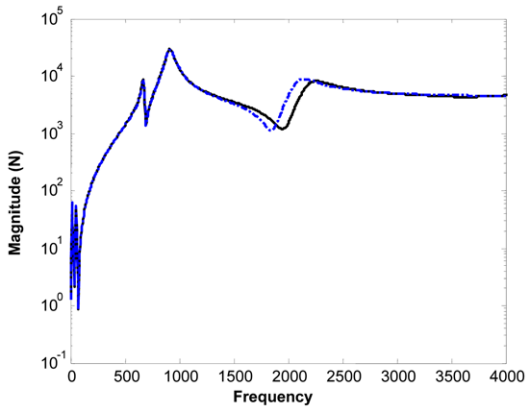

Figure 11. Comparison of the predicted dynamic mesh forces applying the dynamic finite element model (solid line ——) and enhanced lumped parameter model (dashed dotted line -------) for case (a) with pinion and gear both overhung mounted and simply supported.

discrepancies that may be caused by the following two reasons: (i) The process to calculate the effective lumped

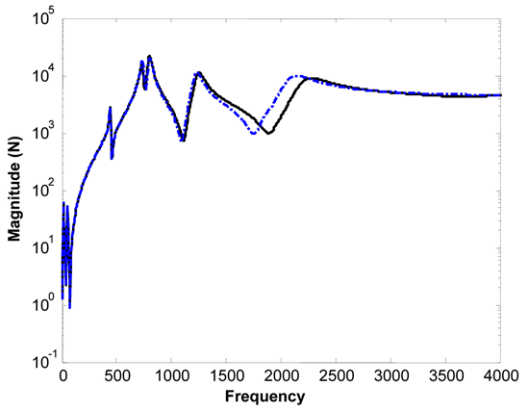

Figure 12. Comparison of the predicted dynamic mesh forces applying the dynamic finite element model (solid line ——) and enhanced lumped parameter model (dashed dotted line -------) for case (b) with pinion and gear both overhung mounted and flexibly supported.

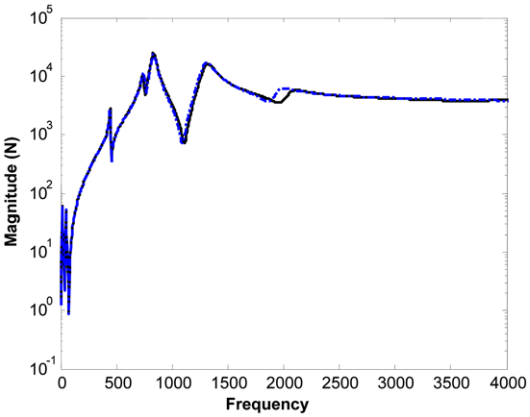

Figure 13. Comparison of the predicted dynamic mesh forces applying the dynamic finite element model (solid line ——) and enhanced lumped parameter model (dashed dotted line -------) for case (c) with pinion straddle mounted, gear overhung mounted and both flexibly supported.

shaft-bearing stiffness and mass and inertia elements may have disregarded the effect of higher order parametric terms leading to minor computational errors; and (ii) Since the newly enhanced lumped parameter synthesis approach is developed based on the first bending mode of pinion and gear, the proposed lumped parameter model cannot accurately predict modes that are coupled to higher pinion or gear bending modes at relatively high frequencies. These neglected higher order bending modes may cause minor residual errors at the predicted frequencies.

5. CONCLUSIONS

In this study, an enhanced lumped parameter modeling approach is proposed to improve the modeling of spiral bevel geared rotor systems without the penalty of using large scale finite element models. The enhancement uses the finite element representation of the gear-shaft assembly to determine the effective mass and stiffness elements at the relevant lumped points. Using this enhanced lumped parameter synthesis approach, the predicted dynamic mesh force function shows excellent agreement with the response calculated by the direct dynamic finite element model. Also, the comparison of the dynamic finite element results to basic lumped parameter calculations in modeling spiral bevel geared rotor system response reveal the limitations of previous approaches. The proposed enhanced lumped parameters retain the efficiency and simplicity of the discretization but still can accurately account for the bending modes of the driving and driven shafts. This is important because the bending modes of the connecting shafts are critical to the dynamical characteristics of the complete spiral bevel geared rotor systems.

REFERENCES

Cheng, Y. (2000). *Dynamics of High-speed Spiral Bevel and Bevel Geared Rotor Systems*. Ph.D. Dissertation. The Ohio State University.

Iida, H., Tamura, A. and Oonishi, M. (1985). Coupled torsional-flexural vibration of a shaft in a geared system (3rd report). *Bulletin of the JSME*, **28**, 2694–2698.

Karnovsky, I. A. (2003). *Free Vibrations of Beams and Frames*. McGraw-Hill. New York.

Kubur, M., Kahraman, A., Zini, D. and Kienzle, K. (2004). Dynamic analysis of multi-mesh helical gear sets by finite elements. *J. Vibration and Acoustics*, **126**, 398–406.

Liew, H. V. and Lim, T. C. (2005). Analysis of time-varying rolling element bearing characteristics. *J. Sound and Vibration* **283**, **3-5**, 1163–1179.

Lim, T. C. and Houser, D. R. (1997). Dynamic analysis of lay shaft gears in automotive transmission. *Proc. SAE Noise and Vibration Conf.*, Traverse City, Michigan, USA, 739–749.

Lim, T. C. and Li, J. (1999). Dynamic analysis of multi-mesh counter-shaft transmission. *J. Sound and Vibration* **219**, **5**, 905–918.

Lim, T. C. and Singh, R. (1990a). Vibration transmission through rolling element bearings. Part I: Bearing stiffness formulation. *J. Sound and Vibration* **139**, **2**, 179–199.

Lim, T. C. and Singh, R. (1990b). Vibration transmission through rolling element bearings. Part II: System studies. *J. Sound and Vibration* **139**, **2**, 201–225.

Lim, T. C. and Singh, R. (1990c). Vibration transmission through rolling element bearings. Part V: Effect of

distributed load on roller bearing stiffness matrix. *J. Sound and Vibration* **169**, **4**, 547–553.

Lim, T. C. and Singh, R. (1991). Vibration transmission through rolling element bearings. Part III: Geared rotor system studies. *J. Sound and Vibration* **151**, **1**, 31–54.

Ozguven, H. N. and Houser, D. R. (1998). Mathematical models used in gear dynamics—A review. *J. Sound and Vibration* **121**, **3**, 383–411.

Peng, T. and Lim, T. C. (2007c). Coupled multi-body dynamic and vibration analysis of high-speed spiral bevel geared rotor system. *Proc. SAE Noise and Vibration Conf. and Exposition*, St. Charles, Illinois, USA.

Peng, T. and Lim, T. C. (2009a). Effects of assembly errors on spiral bevel gear mesh characteristics and dynamic response. *Proc. JSME Int. Conf. Motion and Power Transmissions*, Sendai, Japan.

Peng, T. and Lim, T. C. (2009b). Influence of gyroscopic effect on spiral bevel and bevel geared system dynamics. *SAE Int. J. Passenger Cars: Mechanical Systems* **2**, **1**, 1377–1386.

Smith, J. D. (2003). *Gear Noise and Vibration*. Marcel Dekker. New York.

Tamminana, V. K., Kahraman, A. and Vijayakar, S. (2007). A study of the relationship between the dynamic factors and the dynamic transmission error of spur gear pairs. *J. Mechanical Design* **129**, **1**, 75–84.

Vedmar, L. and Andersson, A. (2003). A method to determine dynamic loads on spur gear teeth and on bearings. *J. Sound and Vibration* **267**, **5**, 065–1084.

Vijayakar, S. M. (1991). A combined surface integral and finite element solution for a three-dimensional contact problem. *Int. J. Numerical Methods in Engineering* **31**, **3**, 525–545.

Vijayakar, S. M. (2003). *Hypoid Face Milled User's Manual*. Advanced Numerical Solutions LLC.

Vinayak, H., Singh, R. and Padmanabhan, C. (1995). Linear dynamic analysis of multi-mesh transmissions containing external rigid gears. *J. Sound and Vibration* **185**, **1**, 1–32.